JOURNAL OF GEOPHYSICAL RESEARCH, VOL. 103, NO. A1, PAGES 135–150, JANUARY 1, 1998

Flux rope structures in the magnetotail: Comparison between Wind/Geotail observations and global simulations

R. M. Winglee,[1] S. Kokubun,[2] R. P. Lin,[3] and R. P. Lepping[4]

Abstract. On December 11, 1994, Geotail observed several reconnection (negative B_z) events at a position 30-40 R_E down the tail over a 24 hour period. This period is also interesting because the solar wind conditions were well monitored by Wind, which was only about 20 R_E in front of the bow shock, and because IMP 8 was at nearly the same x value as Geotail, but at high latitudes. Global fluid simulations that incorporate higher-order corrections to Ohm's law are used to produce a three dimensional picture of the reconnection site in conjunction with the Geotail data. It is shown that many of the negative B_z events have appreciable core magnetic fields, which in the modeling appear to form around 20 R_E about 10 min earlier than observed by Geotail. The predicted time of the formation coincides approximately with increased ionospheric activity observed by the Canadian Auroral Network for the OPEN Program Unified Study (CANOPUS) magnetometer chain. The flux ropes also appear to be highly localized (2-4 R_E), particularly in x and z when they are first created. In addition, they have a distinctive bipolar core magnetic field, but the probability that a spacecraft observes a unidirectional or bipolar signature is highly dependent on the position of the center of the current sheet relative to the spacecraft. Bipolar signatures are predicted to be most easily seen when the spacecraft is near the center of the current sheet, while unidirectional signatures are most likely to be observed at more distant encounters.

1. Introduction

The evidence for magnetic reconnection having an important role in the development of substorms comes from the frequent observation of negative B_z in the tail in association with substorm onset [*Hones*, 1976]. In the near-Earth neutral line model of *Hones* [1979], the center of the plasmoid was envisaged to have a weak magnetic field where an O-type neutral point forms. However, subsequent studies have shown that the structure of the plasmoid can be very much more complicated with strong core magnetic fields being present [*Sibeck*, 1984; *Elphic et al.*, 1986; *Slavin et al.*, 1989; *Sibeck et al.*, 1990; *Moldwin and Hughes*, 1991, 1992]. On occasion, the core magnetic field can be as strong as, and in some cases exceed, the lobe magnetic field [*Slavin et al.*, 1995]. The direction of the core magnetic field is usually (34 out of 39 cases) in the direction of the B_y component of the interplanetary magnetic field (IMF) [*Moldwin and Hughes*, 1992]. The core field is also observed to be generally unidirectional, although on occasion bipolar B_y signatures are seen in conjunction with bipolar B_z signatures [*Moldwin and Hughes*, 1992].

Initial estimates for the average diameter of the flux ropes by *Moldwin and Hughes* [1992] suggested that they were of the order of 10 ($\pm$6) R_E in the near-tail region. Further down the tail they appear to expand to about 16 R_E in the midtail region and to about 19 R_E in the distant tail. More recently, *Lepping et al.* [1995, 1996] have used a force-free model for flux ropes to obtain size estimates for flux ropes observed by Geotail and ISEE 3, respectively. They found that in both the midtail to distant tail regions the average diameter was about 10 R_E but in several instances the diameter could be as small as 1-3 R_E.

The distinctive signatures of these flux ropes can provide important insight into the processes driving magnetic reconnection, and hence improve our understanding of substorm triggers. The importance of the B_y component of the IMF in the formation of flux ropes has been demonstrated by the regional MHD models of *Birn and Hesse* [1990] and *Fu et al.* [1990], where a uniform B_y is imposed on model magnetotail configurations. Global MHD models [*Ogino et al.*, 1990; *Kivelson et al.*, 1996] have demonstrated flux rope generation in the presence of a non-zero B_y component of the IMF. However, such models cannot explain the

[1]Geophysics Program, University of Washington, Seattle.
[2]STELAB, Nagoya University, Tokyokawa, Japan.
[3]Space Sciences Laboratory, University of California, Berkeley.
[4]NASA Goddard Space Flight Center, Greenbelt, Maryland

Paper number 97JA02415.
0148-0227/98/97JA-02415$09.00

occasional presence of bipolar flux ropes or flux ropes with opposite polarities to IMF B_y. In addition, the flux ropes generated in both the regional and the global MHD models are about 20 R_E in width along x, which is significantly larger than indicated by the above observations.

The generation of flux ropes/plasmoids is integrally related to the question of how reconnection is produced in a collisionless plasma. In ideal MHD the magnetic field is frozen in, but in numerical simulations when the tail current sheet thins to a few grid points, grid point or numerical reconnection occurs, irrespective of the numerical algorithm. In other words, there is no intrinsic scale size except for some arbitrary grid spacing. The introduction of an anomalous resistivity can remove numerical reconnection but in itself introduces a new arbitrary parameter.

There are several suggestions that the reconnection rate is determined by particle processes when the current sheet becomes sufficiently thin. *Drake et al.* [1994] have shown for idealized geometries that reconnection does not occur in the smooth MHD manner but rather occurs through filamentation and kinking of the current sheet. *Biskamp et al.* [1995] identified the Hall term in the generalized Ohm's law as playing an important role in controlling the reconnection rate in collisionless plasmas. *Ma and Bhattacharjee* [1996] have also found a similar result but using a fluid code that incorporates the full form of the generalized Ohm's law. Particle effects have also been shown to be important in determining the reconnection rate in the magnetotail [*Winglee and Steinolfson*, 1993; *Steinolfson and Winglee*, 1993] and magnetopause [*Winglee*, 1994]. In particular, due to finite ion gyroradius effects, there is differential convection of ions and electrons across the current sheet which can in turn lead to the formation of field-aligned currents that divert current out of the current sheet and allow reconnection to occur. In so doing, these currents can produce the strong core magnetic fields associated with reconnection events.

More recent three-dimensional (3-D) particle simulations by *Zhu and Winglee* [1996] of the Harris current sheet configuration have shown not only that particle effects lead to field-aligned currents but that the current sheet becomes kink unstable and flux ropes are generated during reconnection. The core field can be comparable to the lobe magnetic field. *Pritchett et al.* [1996] have confirmed these results but have suggested that the core magnetic field is extremely weak when a normal magnetic field component is present. However, these later simulations do not include an ionosphere, and the development of field-aligned currents that support the core field are easily affected by the different choices of boundary conditions possible in such codes.

While the above particle treatments show that the reconnection rate is controlled by inherent kinetic processes, placing particle processes into the global context is very difficult and quantitative verification has not been made. On the other hand, global MHD simulations rely on either unphysical or arbitrary processes to drive reconnection, and while they qualitatively produce observed reconnection signatures, quantitative verification has also not been achieved.

The purpose of this paper is twofold. First, we seek to incorporate some of the above kinetic processes into the global context. Our method is described in section 2 and utilizes grid resolution of 0.33 R_E near the reconnection site, at which point particle effects first become appreciable. It is shown in section 3 that by incorporating such processes we are able to reproduce the flux rope structures seen in the kinetic particle simulations of *Zhu and Winglee* [1996] except that the treatment here is fluid and artificial mass ratios do not have to be assumed. It should be noted that there could still be additional processes at even smaller scale lengths that could produce further modifications to the reconnection rate [*Drake et al.*, 1994; *Biskamp et al.*, 1995; *Ma and Bhattacharjee*, 1996].

The second objective is to compare the modeling results with in situ observations through a case study of flux ropes observed by Geotail on December 11, 1994. During this period, Geotail was in the near-Earth region at about 30 R_E down the tail. There was some isolated activity early in the day followed by a period of extended activity in the afternoon. Several flux ropes were observed throughout the day. Using solar wind data from WIND, it is shown that for about half the observed flux ropes the modeled magnetic field was in reasonable agreement with the observed local temporal variations in B_y and B_z (section 3). The flux ropes at their point of origin in the simulations are fairly small with a diameter of a few R_E but expand down the tail to about 10-15 R_E. The plasmoid that surrounds the flux rope typically has a diameter about twice that of the flux rope (sections 4-6). In the disturbed period there are many indicators that even smaller scale processes than are resolved here are important in the reconnection process. A summary of results and their relation to the average properties of flux ropes is given in section 7. The simulations presented here are some of the first where there is quantitative corroboration of modeled magnetic reconnection signatures with in situ observations.

2. Modeling Magnetic Reconnection in the Local and Global Environment

As noted in the introduction, there can be significant differences between the reconnection rate as determined from resistive MHD and particle treatments. This difference is highlighted in Figure 1 where the top panels show two different view angles of a Harris current sheet: the typical side view (Figure 1a), and the view from the Earth across the current sheet (Figure 1a). MHD simulations of this Harris configuration in which a uniform resistivity is assumed produce the classic plasmoid signature where magnetic islands are formed in association with negative B_z. This magnetic island configuration is also seen in particle simulations [*Zhu and Winglee*, 1996], as illustrated in Figure 1c. However, from the cross-tail view (Figure 1d) the particle treatment in-

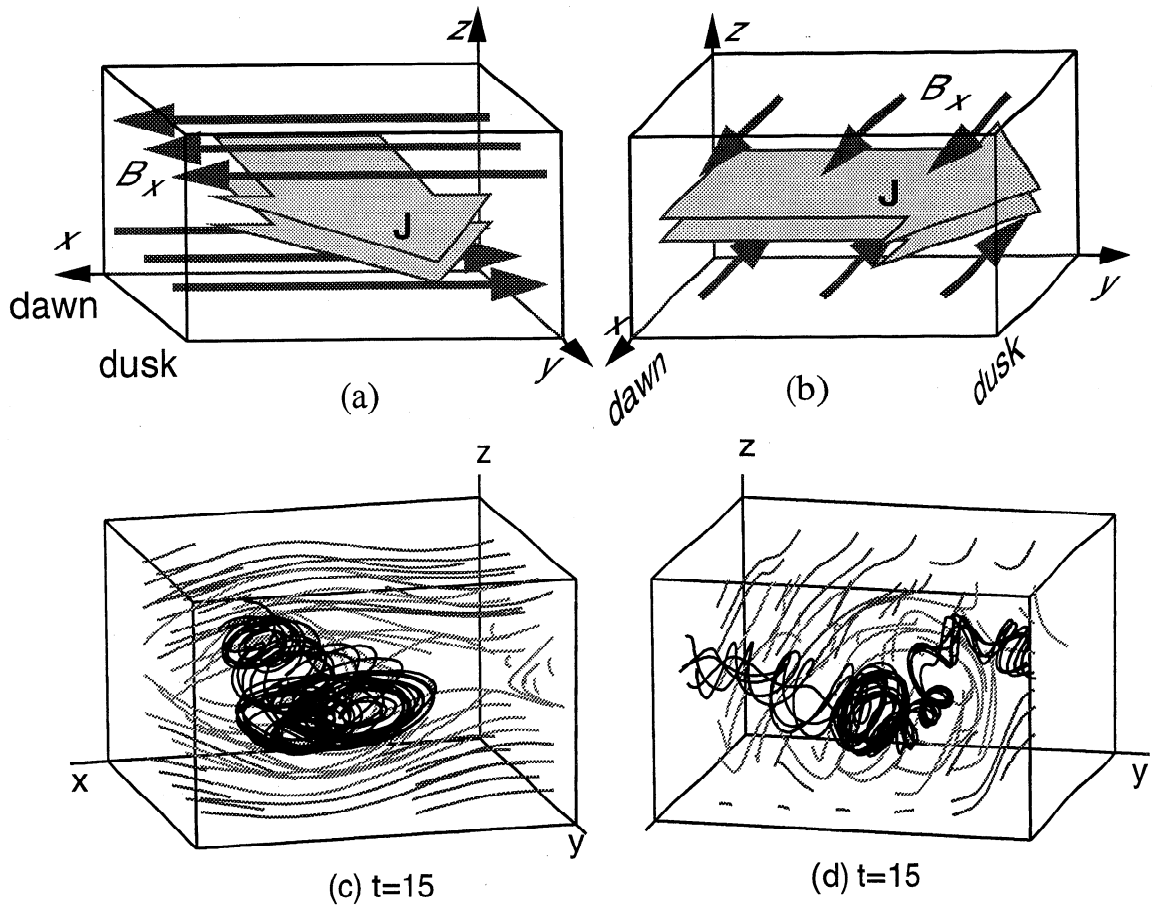

Figure 1. Two different views of a Harris current sheet. The left hand side shows a side view while the right shows the view from the Earth. The particle simulations (bottom panels) from *Zhu and Winglee* [1996] show that while magnetic island will be produced in a similar fashion to resistive MHD, the center is not an O-neutral point but is instead threaded by a flux rope that can cross much of the tail.

dicates that the magnetic island is not the O-neutral point of MHD but rather is threaded by a flux rope.

The core magnetic field arises because the electrons with their small gyroradius can convect more easily into the center of the current sheet than the ions, i.e., the electrons remain magnetized over a larger region. As the current sheet starts to tear or clump, these differing charge distributions start to move along the x axis, which sets up the field-aligned currents that generate the B_y core magnetic fields. These field-aligned currents produce a current diversion from the tail current sheet and with the resistance of the ionosphere produce an effective resistivity on the tail current sheet allowing reconnection to occur.

In order for a global model to provide a reasonable comparison with in situ observations of reconnection events, some of these local particle processes have to be incorporated into the global environment. In order to do so, we retain higher-order corrections to the plasma dynamics and the generalized Ohm's law that more accurately reflect the ion and electron dynamics. In particular, the full form of the plasma equations of motion are given by

$$\frac{\partial \rho}{\partial t} + \nabla \cdot (\rho \boldsymbol{V}) = 0 \tag{1}$$

$$\rho \frac{d\boldsymbol{V}}{dt} = -\nabla P + \boldsymbol{J} \times \boldsymbol{B} + \rho_q \boldsymbol{E} \tag{2}$$

$$\frac{\partial}{\partial t}\left(\frac{1}{2}\rho \boldsymbol{V}^2 + \frac{P}{(\gamma-1)}\right) + \nabla \cdot \left(\boldsymbol{V}\left(\tfrac{1}{2}\rho \boldsymbol{V}^2 + \tfrac{\gamma P}{(\gamma-1)}\right)\right) = \boldsymbol{J} \cdot \boldsymbol{E} \tag{3}$$

$$\frac{\partial \boldsymbol{B}}{\partial t} = -\nabla \times \boldsymbol{E}\,. \tag{4}$$

The space-charge density ρ_q is given by

$$\nabla \cdot \boldsymbol{E} = \frac{\rho_q}{\epsilon_0} \tag{5}$$

and is in general small but is retained for self-consistency. At this stage the equations are exact in the sense that there is no loss of information from the full two-fluid equations. The space-charge term is also retained because when necessary it is used to calculate the magnetospheric potential which is obtained by inverting Poisson's equation [cf. *Winglee et al.*, 1997a],

$$\nabla^2\phi = -\frac{\rho_q}{\epsilon_0} . \quad (6)$$

Approximations must be made when the displacement current in Ampere's law is neglected so that $\mu_0 \boldsymbol{J} = \nabla \times \boldsymbol{B}$. In order to close the equations, an Ohm's law must be adopted. The generalized Ohm's law [e.g., *Krall and Trivelpiece*, 1986] contains all the electron and ion dynamics, including finite electron inertial effects and finite gyroradius effects. However, an exact solution of these equations requires a very small time step in order to resolve electron processes. Thus, approximations of the generalized Ohm's law have to be made to obtain a tractable solution.

Ideal MHD retains the two dominant terms of the generalized Ohm's law, i.e.,

$$\boldsymbol{E} + \boldsymbol{V} \times \boldsymbol{B} = 0 . \quad (7)$$

In this approximation the only electric field generated in the plasma is the convective electric field which is always orthogonal to $\boldsymbol{V}$ and $\boldsymbol{B}$. For this electric field, the electrons and ions move as a single fluid under $\boldsymbol{E} \times \boldsymbol{B}$ drift motion. The configuration of the tail is such that the electric field lies essentially in the direction of the tail current, which is primarily in the y direction.

However, in the plasma sheet boundary layer, there can be additional electric fields in the x-z plane [e.g., *Cattell and Mozer*. 1984] due to the differential penetration or convection of the ions and electrons. These are the same processes that produce the core magnetic field in the particle simulations in Figure 1, and they can be responsible for driving additional currents in the x-z plane, i.e., into and out of the ionosphere. *Winglee* [1994] has shown that these currents can lead to a current diversion from the tail current sheet into the ionosphere. With the latter's resistivity, these additional processes can be thought of as producing an effective plasma resistivity in the magnetotail and an unphysical, anomalous or numerical resistivity is not required to drive the magnetic reconnection.

Incorporation of these processes is most easily obtained by noting that the time step in fluid simulations is of the order of a few seconds. On this timescale, the electrons can travel significant distances along a magnetic field line so that they can be assumed to be approximately steady state, i.e. $D\boldsymbol{V}_e/Dt = 0$, or

$$\boldsymbol{E} + \boldsymbol{V}_e \times \boldsymbol{B} + \frac{1}{en_e}\nabla P_e = 0 . \quad (8)$$

The ∇P_e term in the presence of a nonuniform density, such as at boundary layers, can make contributions to the curl of the electric field, which in turn produces magnetic field and current perturbations. Physically, the gradients in pressure are required to produce the boundary layer/current system, and the gradients in density ensure that the electric fields produced by the differential convection of the electrons and ions are not shorted out by flows from other regions.

The electron momentum equation (8) can be cast into the more usual terms of an Ohm's law by noting that $\boldsymbol{J} = en(\boldsymbol{V}_i - \boldsymbol{V}_e)$ and $\boldsymbol{V} \simeq \boldsymbol{V}_i$. Making these substitutions into (8) the next higher order form of the generalized Ohm's law is obtained with

$$\boldsymbol{E} + \boldsymbol{V} \times \boldsymbol{B} \simeq \left(\frac{\boldsymbol{J} \times \boldsymbol{B}}{en_e} - \frac{1}{en_e}\nabla P_e\right) . \quad (9)$$

A perturbative solution was used by *Winglee* [1994] to show that the higher-order Ohm's law can lead to additional field-aligned currents in the noon-midnight meridian which map into the auroral region, consistent with the currents seen in particle simulations. This perturbative expansion is equally valid in 3-D simulations. However, to avoid any ambiguities that arise from perturbative solutions, the following work is based on an exact solution to (9) with the assumption that the electron pressure P_e is equal to one half of the total plasma pressure, as implicitly assumed in ideal MHD. Note that if the system is in approximate equilibrium (i.e., $\nabla P \simeq \boldsymbol{J} \times \boldsymbol{B}$) then the right-hand side of (9) is of the order of $(1/2)\boldsymbol{J} \times \boldsymbol{B}$ for equal temperatures and of the order of $\boldsymbol{J} \times \boldsymbol{B}$ if the electron temperature is much less than the ion temperature.

In principle the higher order corrections in (9) can give rise to high-frequency/short-wavelength whistlers. These waves are not resolved in the present model (nor are they incorporated in MHD) since they are subgrid size and the restrictions that they might impose on the time step and spatial scales do not appear to be relevant. Comparison with in situ measurements from Geotail and IMP 8 shows that the model is able to produce reasonable agreement with observed magnetic fields in a variety of regions of the magnetosphere [*Winglee et al.*, 1997b,c].

The grid spacing for this case study is variable, with a minimum 0.33 R_E in the inner magnetosphere and 3 R_E in the distant tail. The simulations extend ± 67 R_E on the flanks and 200 R_E into the tail $(-x)$ and 40 R_E upstream of the Earth. For this grid resolution, the above corrections are marginally resolved. However, since the corrections to the ideal Ohm's law in dimensionless units are inversely proportional to the ratio of the grid spacing (Δ) to the ion skin depth (c/ω_{pi}), they can be enhanced by increasing the assumed value of the ratio of the ion skin depth to the grid spacing. In the present case in order to compensate for the limited grid resolution, the ratio is assumed to be 8 of a density of 2 cm^{-3} instead of its actual value of 16 for a pure H^+ plasma. This approximation is actually valid if O^+ is an important component of the plasma.

The inner radius of the simulations is set at 3.5 R_E, which is typical of most global simulations [e.g., *Ogino et al.*, 1990]. Around this inner boundary, a resistive layer is incorporated that acts like the ionosphere. In this region the Ohm's law (9) is modified such that

$$\boldsymbol{E} + \boldsymbol{V} \times \boldsymbol{B} \simeq \left(\frac{\boldsymbol{J} \times \boldsymbol{B}}{en_e} - \frac{1}{en_e}\nabla P_e\right) + \eta_{iono}(r)\boldsymbol{J} . \quad (10)$$

Note that while only a scalar resistivity is incorporated in (10), the actual conductivity is a tensor when the

retention of the Hall term is taken into account. By assuming that the magnitude of η_{iono} decreases rapidly with radial distance (in practice it is only significant within three cells of the inner radius), the Ohm's law allows a smooth transition from the collisional plasma of the ionosphere to the collisionless plasma of the magnetosphere. Placing the resistive layer inside the simulation system also has the advantage that the resistivity along the current path is not fixed, but rather can float since the current can close at different altitudes depending on the forcing from the solar wind conditions.

The other feature of the ionospheric resistivity is that it is allowed to vary with both latitude and longitude consistent with (1) daylight ionization and (2) enhanced ionization from particle precipitation. For the daylight component the ion-neutral collision frequency at the inner radius is assumed to equal the ion cyclotron frequency at the equator, and then to decrease to 1/10 of this value at the day-night terminator. The nightside collision frequency is assumed to be constant at 1/10 of the ion cyclotron frequency. Superimposed on this component, an additional component is added that is centered at 65° magnetic latitude with a half width of 5°. This component, which represents ionization from particle precipitation, has a peak ion-neutral collision frequency that is set equal to the ion cyclotron frequency. Experiments with different forms of resistivity show that the magnetospheric configuration is insensitive to the actual form of the resistivity imposed on the system, except possibly for the shape of the potential at midlatitudes.

Tests with various forms of the resistivity show that the cross-polar cap potential is not very sensitive to the resistivity model in that doubling the resistivity produced changes of about 20% in the magnetospheric potential. The auroral current shows somewhat different behavior in that it is also insensitive to changes up to the above assumed values. Above this threshold, further increases in resistivity started to produce faster declines in the current than seen in the potential.

In addition, a dense (200 cm^{-3}) plasma is assumed. The density of this component then falls off as $1/r^5$. This plasma in many ways acts like the ionosphere by providing a sink for energy flowing in from the magnetosphere. At the same time it provides a source of plasma that can be used to populate the tail, as it shrinks and grows with activity.

The model is driven by solar wind conditions observed by Wind. These observations are discussed in the next section. The simulation model was first run for 2 hrs real time with plasma densities and IMF conditions that were representative of the conditions at the beginning of the day. This period allows the magnetosphere to come to approximate equilibrium with the prevailing solar wind conditions. After this period, the simulations were run with the continuously varying solar wind and IMF conditions observed by Wind. The response of the magnetosphere was monitored and the results compared with that observed by Geotail, which was moving through the plasma sheet in the midtail region.

3. Observations

3.1. Solar Wind Conditions

The solar wind conditions as observed by Wind on December 11, 1994, are shown in Figure 2. The observations were taken when Wind was inbound during a perigee pass, starting at 39 R_E upstream and ending at 25 R_E (GSM coordinates). This day is interesting in that it includes periods when the B_z component of the IMF is approximately steady for several hours, followed by periods of disturbed IMF. In particular, the B_z component was primarily northward up to about 1100 UT, although there were a few southward excursions observed around 0200, 0240, 0400, 0700, and 0800 UT. From about 1100 UT to 1600 UT the B_z component was zero on average while between 1600 and 2030 UT the IMF was predominantly southward. After 2030, there was a 1.5 hr period of strong northward IMF followed by a 1.5 hour period of southward IMF.

The period is also of interest because for most of the day the B_y component was primarily negative, except for a 3 hour interval between 1600 and 1900 UT. These extended periods of positive or negative IMF B_y can be used to look for differences in the signatures of the flux ropes in the magnetotail.

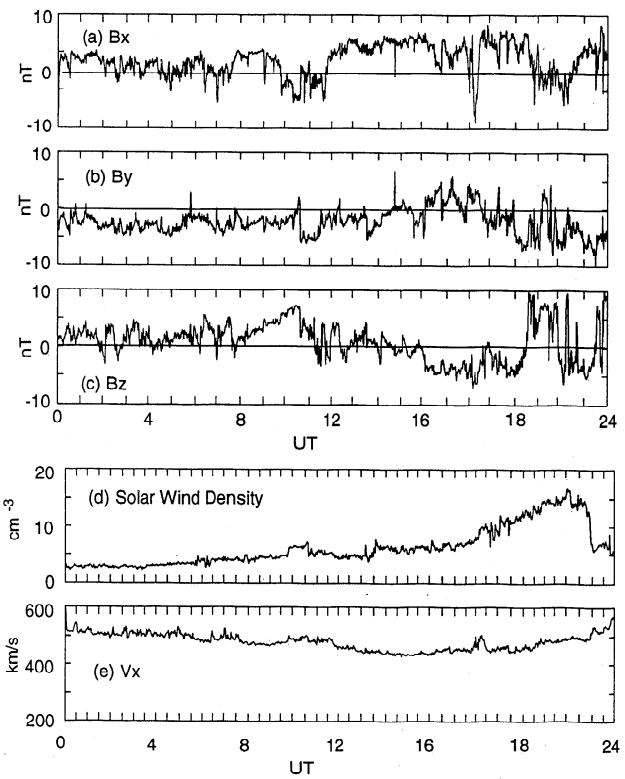

Figure 2. Solar wind conditions observed by Wind on December 11, 1994. The IMF between 0000 and 1100 UT is on average northward except for small southward excursions. Between 1100 and 2100 UT the average B_z IMF decreases to zero or southward, after which there is a strong 90 min excursion northward followed by a similar southward excursion. The solar wind density is slowly increasing during the day.

The solar wind speed throughout the day was approximately steady at 500 km/s. The density was also steady during the first half of the interval, at about 5 cm^{-3}. However, during the second part of the day the density slowly increased, reaching a peak of 15 cm^{-3}. The corresponding solar wind ram pressure increased by a factor of 3 from the beginning of the day to the end.

3.2. Magnetospheric/Ionospheric Activity

The magnetospheric activity as observed by Geotail is shown in the top panels of Figure 3. Geotail was in the midtail region at (-32, 14, -2) R_E (GSM) at the beginning of the day and moved down the tail to (-42, 8, -4) R_E at the end of the day. Geotail was initially in the northern hemisphere (as seen by the positive B_x) and then moved into the southern hemisphere at about 0500 UT. Starting around 1600 UT, Geotail appears to make several excursions into the center of the current sheet, as evidenced by the very small magnitude of B_x.

There are several small (-1 nT) negative B_z events indicating thinning of the current sheet. It is shown in the following that these events, which are often overlooked, are still very important and may be signatures of the formation of a shallow near-Earth neutral line (i.e., a "Y" neutral line as opposed to an "X" neutral line). In addition, there are several stronger (-5 nT) negative B_z events which appear after about 1500 UT as indicated by the arrows. These events are the ones more typically identified with reconnection events. In the present case, many of them are associated with strong (5 to 10 nT) B_y core fields, indicating that they may be flux ropes. The first of these flux ropes is unusual in that it occurs prior to the strong southward turning of the IMF and it has a dipolar B_y core magnetic field. The other flux ropes have the more typical unidirectional B_y core magnetic field. All of these core fields are negative, similar to the predominant B_y component of the IMF. However, it should be noted that the flux ropes observed at 1800 UT have a negative B_y during a time when IMF B_y was positive on average for the preceding 2 hours.

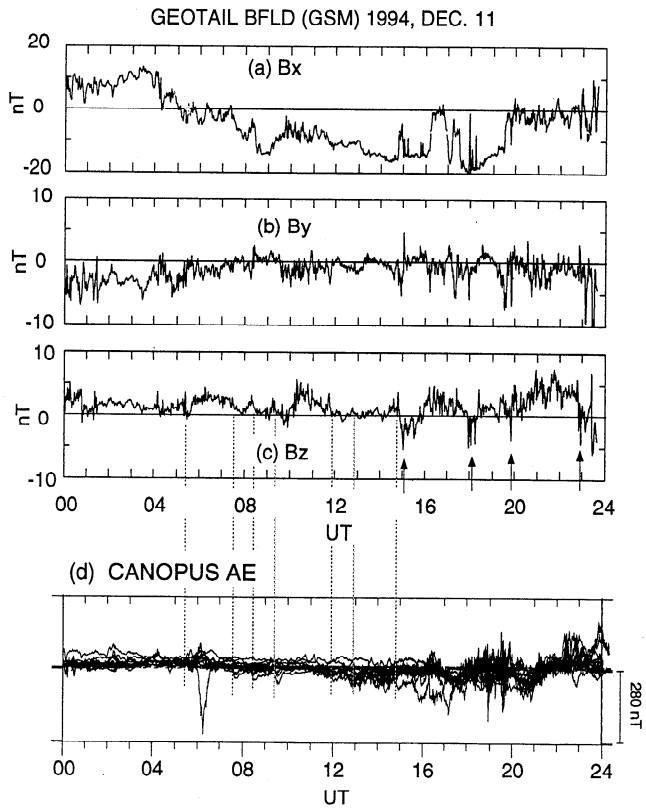

Figure 3. Top panels (Figures 3a, 3b, and 3c) show the magnetic field observed by Geotail as it was outbound moving from x = -32 R_E to -42 R_E. Several negative B_z events were observed during the day, with some of the larger magnitude events (indicated by arrows) appearing when the B_z IMF in Figure 1 decreased on average to zero or southward. Many of the events are associated with strong core fields, and with preceding auroral activity in the CANOPUS data as indicated by the vertical lines.

As a measure of the ionospheric activity, a local AE index was constructed by superposing the B_x perturbations observed by the Canadian Auroral Network for the OPEN Program Unified Study (CANOPUS) magnetometer chain, as shown in the bottom panel of Figure 3. It is seen that even the small negative B_z events observed by Geotail are accompanied by perturbations in the magnetometer data, particularly those around 0530, 0750, 0830 and 0930 UT. It is of particular importance that the ionospheric activity typically seems to increase about 10 min earlier than the appearance of the negative B_z signature seen at Geotail as indicated by the dotted vertical lines. This timing is most easily seen in the negative B_z events between 0700 and 1000 UT.

After 1100 UT, there is a steady overall increase in ionospheric activity in association with the IMF B_z going to zero or negative. Because of the overall increase in activity, it is not easy to ascertain any direct correlation between the large negative B_z events and the ionospheric disturbances.

4. Modeled Magnetotail Response

Figure 4 shows the modeled magnetic field at Geotail (dashed lines) relative to the observed magnetic fields (solid lines). From the magnitude and sign of B_x, it is seen that the Geotail data indicate that the spacecraft was initially in the northern hemisphere, and entered the current sheet between 0400 and 0800 UT. Geotail then stayed in the southern hemisphere until about 1900 UT where it again encountered the current sheet, before moving into the northern hemisphere around 2300 UT. The model results approximately track the entry of Geotail into the sheet, but it occurs later, between about 0600 UT and 1000 UT. Geotail's entry into the southern hemisphere also appears late in the model, at 1200 UT. This delay corresponds to 1.5 R_E in Geotail's z position. The early reentry into the northern hemisphere at 2100 UT also appears to be consistent with the current sheet being about 1.5 R_E lower in z than was actually observed. Such a difference in position occurs because the current sheet is highly warped in the

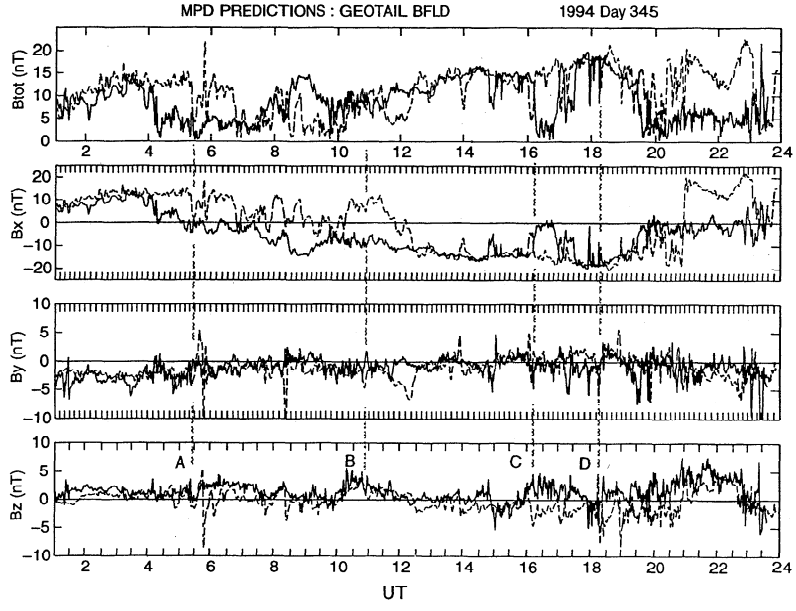

Figure 4. The magnetic field predicted by the simulations (dotted lines) compared with the Geotail observations (solid line). Crossings between northern and southern hemispheres are seen as changes in sign of B_x. The simulations appear to predict that the current sheet is lower by about 1.5 R_E than in reality, which causes it to appear fractionally longer in the northern hemisphere. The overall B_y approximately tracks the observations, as does B_z except that the recovery phases after some of the negative B_z events appear fractionally slower than observed. The vertical dashed lines indicate times of the four case studies examined in detail in later sections.

presence of strong dipole tilt (more than 30° during the day) and strong IMF B_y, with inhomogeneities in the solar wind, particularly during the increasing solar wind dynamics pressure, producing additional twisting of the tail.

The model B_y component tracks the Geotail observations in the sense that it starts at a few nanoteslas negative at the beginning of the day, after which it decreases to an average value of approximately zero. There are several spikes in the simulations in agreement with the observations, particularly at 1600, 1800 and 2000 UT. However, on occasion there are B_y spikes that are predicted and not observed (e.g. at 0600, 0800 and 1200 UT) or vice versa (e.g. 1700 and 1900 UT). The fact that Geotail observes many more B_y spikes in the second half of the interval relative to the first half of the day indicates that the tail in the later interval has become very turbulent or has a lot of fine scale structure and the model at best sees only a small fraction of these smaller scale processes.

The model B_z component also approximately tracks the overall trend in the data, but there are occasions when the model predicts enhanced negative B_z signatures at 0600 and 1600-1900 UT. There are several reasons for these discrepancies. One possibility is that the recovery rate of the simulations after a reconnection event is not fast enough. For example, the model tracks the small negative B_z event at 0530 UT, but shows an additional reconnection event at 0545 UT, whereas the Geotail observations show a steady dipolarization. Therefore the following comparisons will focus on initiation processes when the predicted tail configuration at the beginning of individual events appears to be consistent with the observations. Four such examples, as indicated by the vertical dashed lines in Figure 4, are presented in the following sections.

The data are also of interest because there was simultaneous high-latitude monitoring of the tail by IMP 8, which was at (-34,1, 21) R_E at the beginning of the day and (-34,-12,16) R_E by the end of the day. The comparison between the observations and simulations is shown in Figure 5. There are data gaps between 0300 and 0330 and between 0900 and 1630 UT. It is seen that despite all the activity at Geotail, the observations at IMP 8 are relatively quiet and the global simulations do an excellent job in tracking all three observed magnetic field components. The largest fluctuations between 1800 and 2200 UT are actually associated with IMP 8's approach of the magnetopause as the solar wind dynamic pressure increases. A magnetopause crossing occurs in association with the large spike in $\boldsymbol{B}$ seen around 2130 UT. The fact that IMP 8 does not see any of the current sheet disruption and/or tail flapping implies that the reconnection processes are fairly localized at this distance down the tail.

It is for this reason that the simulations can easily track the IMP 8 data but show more discrepancies at Geotail's position. Furthermore, the agreement with the lobe fields observed by IMP 8 suggests that the differences in the model B_x at Geotail are due to a small offset in z rather than in the strength of the current sheet. As such, in the following, the discussion will

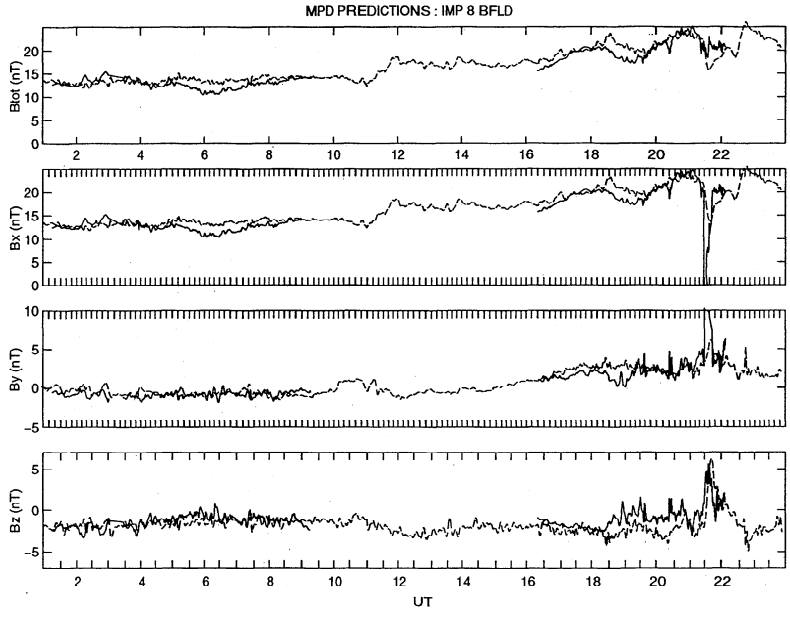

Figure 5. Corresponding comparison with IMP 8 which was at high latitudes and moving toward dawn from (-34,1, 21) R_E to (-34,-12,16) R_E. There is a data dropout between 0900 and 1600 UT. The model predictions are in good agreement with the observations, including the magnetopause crossing at 2130 UT. The fact that IMP 8 has almost the same x and y as Geotail but does not see the same level of activity implies that the negative B_z events observed by Geotail have a limited extent in z.

concentrate on the B_y and B_z signatures that are important in determining the structure along x. The B_x data can always be read off Figure 4.

In the following section, we examine the magnetic signatures that are reasonably captured by the global simulations to provide a three-dimensional (3-D) picture of the formation of plasmoids and flux ropes at higher time resolution. These comparisons can be used to establish the relevant scale sizes and apparent source location relative to Geotail. We will show that the structures are indeed localized, with the likelihood of even smaller-scale structures being present.

5. Modeled Structure of Flux Ropes and Plasmoids: Isolated Events

As an example of the modeled shape of the magnetic field structure during a possible flux rope event, Figure 6a shows the B_y and B_z fields observed by Geotail at 1 min resolution (solid lines) and modeled by the simulations (dashed lines). It is seen that in both cases there is a slow rise in B_z in the first half of the period with B_z reaching a local maximum between about 0521 and 0523 UT. At the same time, B_y on average is slowly increasing but then experiences a large negative excursion around the time of the local maximum in B_z. After this excursion, the observed B_y essentially vanishes while B_z rapidly decreases to near-zero and is even slightly negative for short periods. This event is externally triggered in that it is associated with the southward IMF between 0410 and 0440 UT

The lower panels in Figure 6 show the 3-D mapping of the magnetic field lines. The sphere in the panels indicates the inner radius of the simulations, i.e., 3.5 R_E. The solar wind field lines appear on the left with the curvature on the earthward side being due to their contact with the bow shock. The thin solid lines indicate closed terrestrial field lines, while the dotted indicates reconnected field lines. The instantaneous Geotail field line is shown as a thick solid line. It is seen from the reconnected field lines that there is a shallow (small negative B_z) neutral point existing near the center of the current sheet even at early times. However, this neutral region has only a limited extent in y across the tail.

Enhanced reconnection produced by the southward IMF is seen on the duskside in Figure 6c at about $x = -20$ R_E, and creates a field line/flux rope that threads through the dusk side and into the midnight section of the current sheet. However, the portion of the field line around Geotail has not been affected by the reconnection at this time. This reconnection event is limited in spatial scale to less than 4 R_E in half width both across (z) and along (x) the tail when it is first noticeable. This estimate should be considered an upper limit since the observed B_y and B_z transients appear for a shorter interval than in the simulations. The development of this small-scale flux rope through the center of the magnetic island is very similar to the results from the particle simulations in Figure 1.

The flux rope (and associated reconnected field lines) is seen to move down the tail in Figure 6d with Geotail now appearing on a reconnected field line. Its structure is similar to the classical picture of plasmoids in

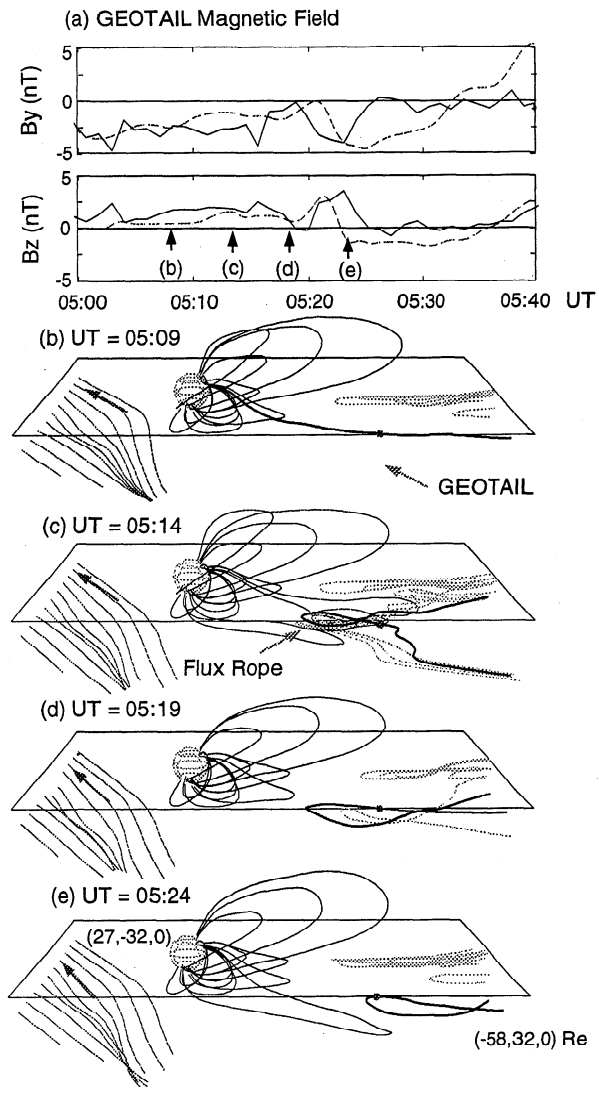

Figure 6. Model reconstruction of a possible flux rope event. (a) Time histories with the Geotail observations indicated by the solid line and model predictions by the dashed line. The simulations show similar features to the observations, including a surge in B_y around 0522 UT in conjunction with B_z vanishing or even turning slightly negative. (b-e) The field line mapping with the solar wind field lines on the left. Closed terrestrial field lines are indicated by the thin black lines while reconnected field by dotted lines. The thick black line gives the instantaneous Geotail field line. A shallow neutral line is seen localized to the center of the current sheet. The flux rope is initiated on the dusk flanks at about $x \simeq -20\ R_E$ at 0514 UT, which is about 10 min before it is actually observed at Geotail.

that B_z is positive on the tailward side so that B_z increases when the flux rope is first encountered. Only when the earthward portion is encountered does the B_z component become negative. The formation of the flux rope earthward of Geotail about 10 min before its observation at Geotail is seen with essentially all the flux ropes in the simulations. This formation time is approximately simultaneous with the beginning of the enhancements in activity in the CANOPUS data discussed in Figure 3.

The origin of the reconnection event can be seen in Figure 7, which shows B_z in the Sun-Earth plane through Geotail's position. The lobes are seen as regions of negative B_z associated with the flaring of the magnetotail. B_z in the plasma sheet is primarily positive except for an earlier reconnection event which appears as the bipolar B_z pair between 50 and 80 R_E in Figure 7a. The IMF is just completing a transition from southward to northward. Because of the presence of a positive B_x in the IMF and the dipole tilt, B_z is more negative in the southern hemisphere than in the northern hemisphere (Figure 7a). This negative B_z from the southern lobe is seen to enter the center of the current sheet (Figure 7b) which generates the flux rope in Figure 5c. The tracing of the negative B_z from the dayside into the nightside suggests that the flux rope in this case is externally triggered.

The corresponding evolution of B_y is shown in Figure 8. Because of the strong negative IMF B_y, most of the B_y in the magnetosphere is negative except in the near-Earth region where the terrestrial magnetic field still dominates. B_y in the vicinity of the reconnection site (as indicated by the ellipse in Figure 8b) becomes increasingly negative in the southern hemisphere while becoming less negative in the northern hemisphere. This bipolar change in B_y intensifies (Figure 8c and 8d) as the current sheet reaches its minimum thickness and the reconnection site is ejected down the tail. This B_y component is similar to that described in the particle simulations in section 2 where the differential convection of ions and electrons into the magnetic island leads to field-aligned currents in association with a v_x motion of the islands. In the present case these processes are incorporated through the Hall and ∇P_e terms in Ohm's law. Their effect is the same in that current is diverted from the current sheet into the ionosphere in association with the development of the dipolar B_y field in the center of the magnetic island or flux rope. Note that even though the B_y is dipolar, the trajectory of Geotail is such that it only observes a unidirectional B_y signature.

We shall show in the following that for periods of weaker IMF B_y, the B_y of the leading edge can actually reverse sign, and that depending where the flux rope is intercepted, either a unidirectional or a bipolar signature can be observed. The presence of a bipolar response in B_y to tail reconnection is intrinsic to the higher order corrections retained in the Ohm's law and to particle treatments [*Zhu and Winglee*, 1996]. Only unidirectional signatures are seen in the MHD simulations of flux ropes [e.g., *Birn and Hesse*, 1990; *Ogino et al.*, 1990]. They arise because the reconnection events occur in very thin current sheets where ideal MHD is no longer valid and field-aligned currents near the boundary layer of the current sheet can develop due to the difference in gyromotion between the electrons and ions.

Figure 9 shows another example of externally driven reconnection that is produced by the differential pen-

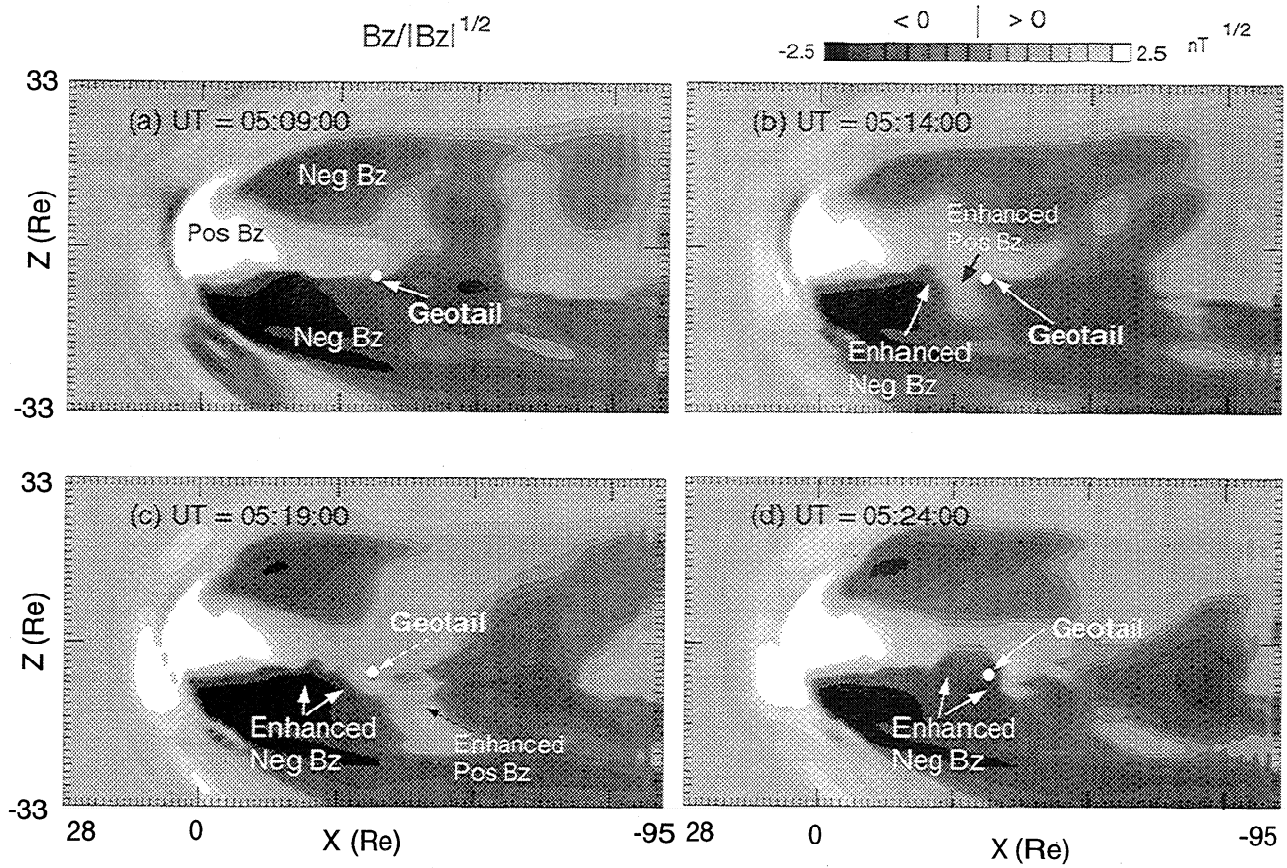

Figure 7. Contours of B_z divided by the square root of the magnitude of B_z. A square root is used so as to emphasize the tail dynamics and deemphasize the inner magnetosphere. The light gray regions indicate positive B_z and dark gray indicate negative B_z. The flux rope event in Figure 6 is produced in association with a northward turning which appears later in the southern hemisphere. This difference in timing causes enhanced convection through the southern lobe which drives the reconnection and produces a traveling compressional wave (TCW) which is led by a region of enhanced positive B_z.

etration of southward IMF into the tail current sheet. The simulation results have been shifted by 5 min which allows the alignment of key features in B_y and B_z. Geotail sees a bipolar signature in B_y reaching a local minimum at 1046 UT and a local maximum at 1055 UT. B_z reaches a local maximum at the time of the negative B_y spike, while it is at a minimum at the positive B_y spike. The simulations show a decline in B_z that essentially matches that observed by Geotail. A negative B_y spike is seen in association with the decline in B_z, but the spike is broader than the observations.

The field line tracing shows that Geotail moves from a closed configuration (Figure 9b) to one which is open in the northern hemisphere (produced by reconnection in the northern hemisphere). The B_y field appears as strong and at times even dominates the B_z component. As a result, the instantaneous Geotail field line passes through the duskside current sheet and exits the current sheet near the noon-midnight meridian. As the field line moves beyond Geotail (Figure 9d), the spacecraft moves into the northern lobe so that the instantaneous field line becomes more typical of open configurations where the field lines map almost parallel to the current sheet. At this time, the B_z at Geotail is at a minimum.

6. Events During a Disturbed Period

As discussed in section 2, during the second half of the day, the average value of IMF B_z declined as the solar wind dynamic pressure was increasing. These conditions lead to a disturbed period of almost continuous activity in the CANOPUS data. It is during this period that several large negative B_z events were observed by Geotail.

The main difference in the tail between the quiet and disturbed periods seen in the modeling is that in the latter a shallow neutral line, where tailward of the neutral line B_z is a few nanoteslas negative forms across much of the tail for most of the time. This configuration more closely resembles "Y" neutral lines rather than "X" neutral lines. External or local processes can enhance or trigger reconnection in the vicinity of this pre-existing neutral line, which can generate enhanced (several nanoteslas) negative B_z signatures in the tail in

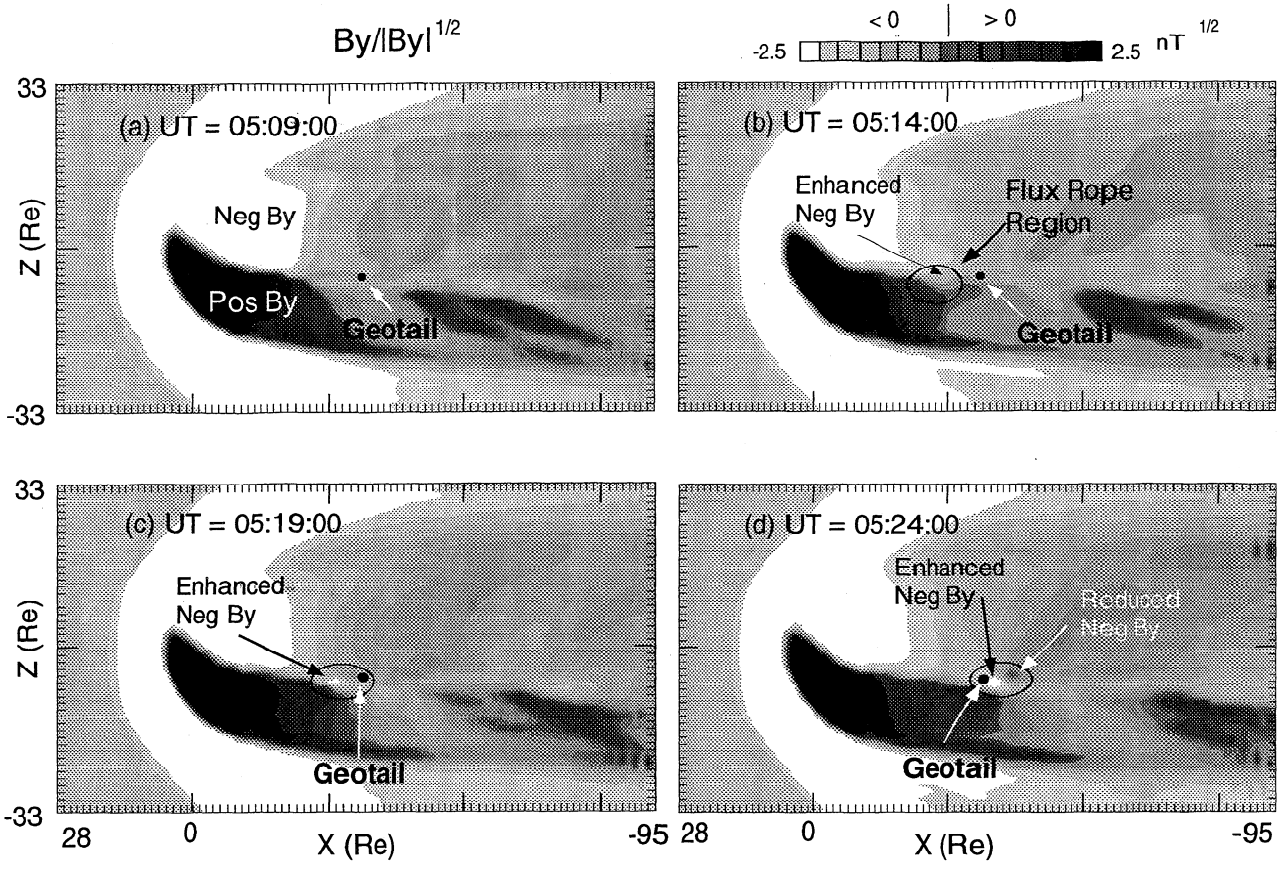

Figure 8. As in Figure 7, but for B_y and the shading scale has been reversed. The flux rope is associated with enhanced negative B_y in the southern lobe while it becomes less negative in the northern lobe (although it actually does not turn positive in the present case). This dipolar pair is characteristic of the flux rope generation in the model and indicates that it is localized with a half width of 2-4 R_E when it first forms. As it moves down the tail it expands to several R_E.

association with the formation of an "X" neutral line. An example of this type of reconnection is illustrated in Figure 10. B_z as seen in the observations is initially slightly negative at 1550 UT. B_z then increases to a local maximum at about 1611 UT, after which it decreases to almost zero for about 10 min before reaching another local maximum at 1625 UT. The simulations follow the overall behavior except that the period between the local maxima is slightly longer at 15 min, and simulation B_z is negative between the maxima. The simulations also include a negative B_y spike around 1612 and 1625 UT, although the positive spike that precedes the negative spike at 1609 UT was not observed.

The presence of the preexisting neutral line can be seen in Figure 10b, where tailward of Geotail there are several reconnected field lines. A flux rope/plasmoid is starting to form earthward of Geotail. The difference between this configuration and those in Figures 6 and 9 is that earthward of Geotail there are many reconnected field lines that occupy a significant fraction of the width (in y) of the current sheet. The leading edge of the flux rope starts to reach Geotail in Figure 10c, while the trailing edge reaches Geotail some 5 min later. The flux ropes produced at this time show a much stronger helical structure than the earlier events.

Despite these differences the results are similar to those in Figures 6 and 9 in that (1) the leading edge has an enhanced positive B_y which is in the opposite sense to the B_y of the IMF, while the trailing edge shows a negative enhancement, (2) the reconnection occurs about 10 min before the negative B_z signatures are seen at Geotail, and (3) they are associated initially with small-scale structures. The fact that the B_y structure of the flux rope is approximately independent of IMF B_y is due to the fact that the B_y of the flux rope is locally generated by the Hall and ∇P_e term corrections (i.e., by particle processes), and that not all the flux rope structure needs to be generated by external IMF conditions.

The size of the flux rope relative to the plasmoid structure can be seen on comparing Figure 11, which shows contour maps of B_y, and Figure 12, which shows contours of B_z. The flux rope is identified by the dipolar signature in B_y in Figure 11. As noted earlier, the leading edge tends to have a positive B_y while the trailing edge has negative B_y. This bipolar structure is again

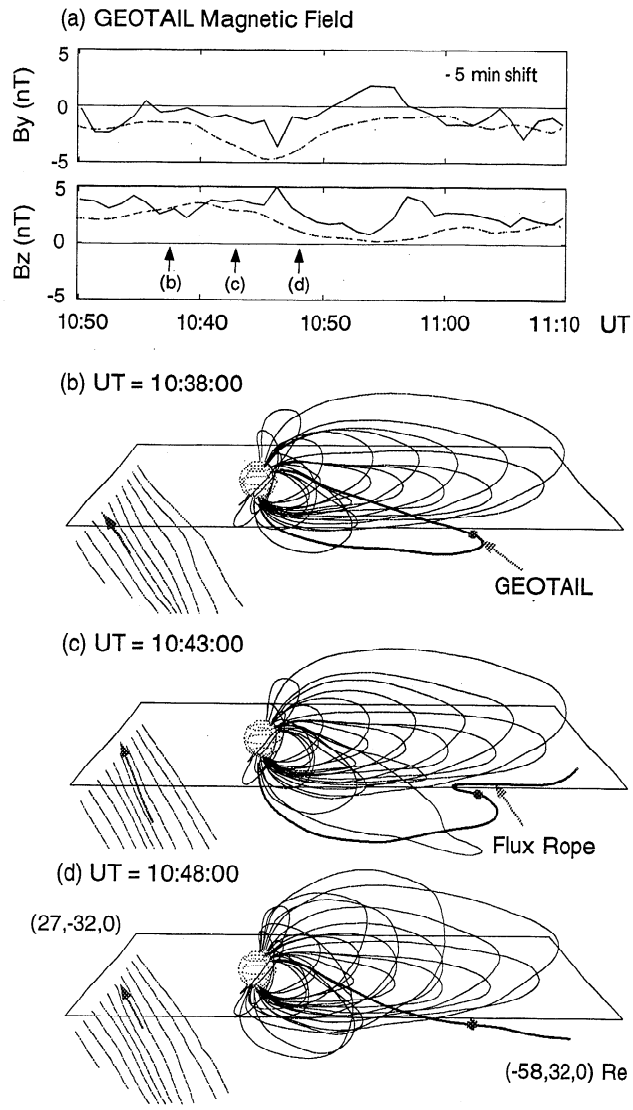

Figure 9. As in Figure 6, but showing the formation of a flux rope with a bipolar signature in the absence of any strong reconnection signatures. Note that the observed B_y perturbation is more localized than predicted by the model, which suggests that actual flux rope structures can be smaller than those seen in the simulations.

highly localized with an initial half width of about 3 R_E along the tail and about 2 R_E in z. The fact that Geotail tends to observe more unidirectional B_y signatures can be explained by the fact that it tends to pass either above or below the center of the flux rope and it is only when it has a near-encounter with the center of the flux rope that a bipolar signature is observed.

The size of the flux rope is seen to expand in both y and z as it moves down the tail, reaching about 10 R_E in width at about 50 R_E down the tail. This value is typical of that inferred from ISEE 3 and Geotail observations [*Slavin et al.*, 1989; *Lepping et al.*, 1995, 1996].

The size of the plasmoid can be estimated from B_z, which is seen initially to become negative in the southern portion of the current sheet (Figure 12a). Eventually, negative B_z penetrates across the full current sheet (Figure 12c). Classifying the region occupied by this negative B_z and the region of positive B_z in the leading edge as the plasmoid (consistent with the magnetic field mapping), it is seen that the plasmoid signature has nearly twice the cross-sectional area as the flux rope signature seen in B_y. However, even with its larger cross-section area, the plasmoid is of insufficient size to make significant perturbations at IMP 8, which has approximately the same x as Geotail but has a relatively large $z \simeq 18\ R_E$.

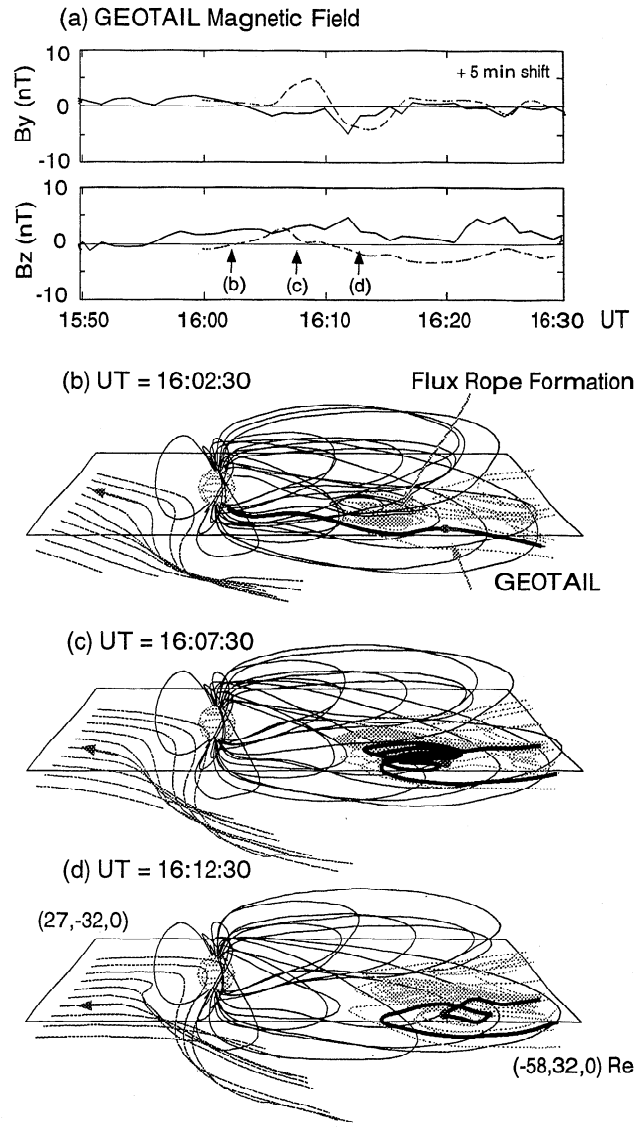

Figure 10. An example of flux rope generation during a disturbed period. In this case there is a preexisting near-Earth neutral line across much of the current sheet. Both the model and observations show a local minimum in B_z between about 1610 and 1620 UT, although the global model overpredicts the decrease. On the lead edge of this decline in B_z, a negative B_y spike is seen. The field line mapping again shows that the flux rope first appears some 10 min before it is observed.

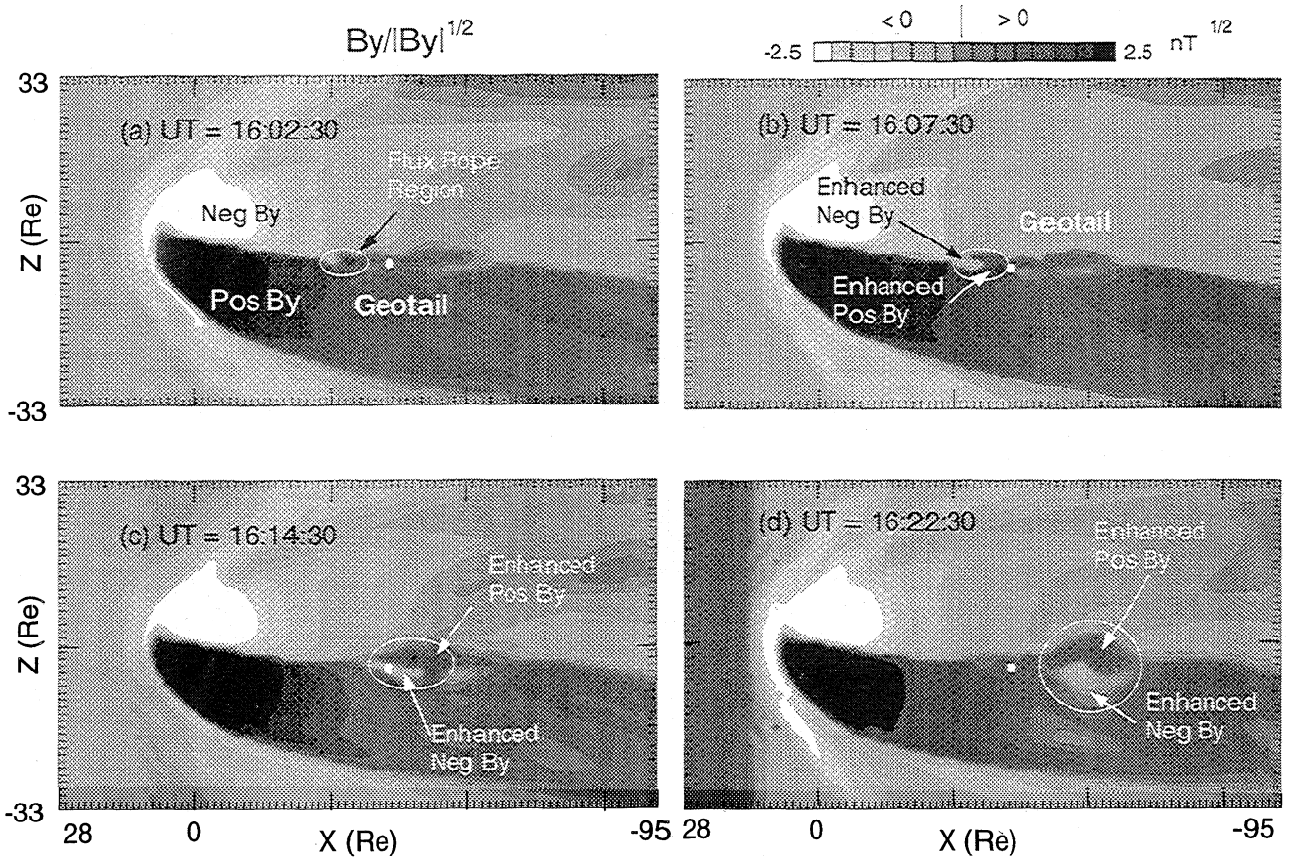

Figure 11. Contours of the B_y associated with the flux rope in Figure 10. The flux rope is easily identified by the dipolar signature, and is seen to expand from a few R_E when it first forms to 10-15 R_E in the midtail region. The actual observed signature depends highly on the position where the spacecraft intercepts the flux rope.

An example of a multiple reconnection event is shown in Figure 13. This event occurs during sustained southward IMF and is a good example of interally triggered reconnection. The observations show three closely spaced negative spikes in B_z that reach a minimum of about -5 nT. The first of these spikes is associated with a strong (-7 nT) B_y spike while the latter two have weak (1 - 2 nT negative) B_y perturbations associated with them. The simulations show a double even, but it appears about 10 min late relative to the observations.

These events are driven by strong southward IMF which forces a shallow neutral line across much of the tail, as seen by the field line tracing in Figures 13b-13d. This configuration is only marginally steady state. When the current sheet is sufficiently thin, the corrections to Ohm's law (9) produce a current diversion out of the tail current sheet that drives the multiple reconnection event on short timescales. Such processes are not seen when the corrections are omitted from Ohm's law.

7. Summary and Discussion

This paper presents a comparison of reconnection signatures from global fluid modeling and in situ observations by Geotail. The common feature throughout all the events is that the reconnection in general occurs on small scales, of the order of only a few R_E at distances between about 20-30 R_E down the tail. On these scale lengths, ideal MHD is not valid and kinetic effects begin to play increasingly important roles. These effects are partially included in a new global treatment that retains the Hall and ∇P_e terms in the generalized Ohm's law. These corrections allow additional electric fields and currents in the $x-z$ plane in the tail. By diverting current out of the tail current sheet, they can produce an effective plasma resistivity on the tail. The word "partially" is used here because it is possible that additional processes down to the electron inertial length can be present and be sufficiently important that they can also modify the reconnection rate.

The modeling shows the development of several negative B_z events within 5 min of when such events were actually observed by Geotail. The model is limited though in that on occasion the model overestimates the negative B_z by about -1 nT and on occasion it misses some of the observed negative B_z events, particularly during the disturbed period in the second half of the day. While the simulations are not perfect, they should be considered an important first step in making quantitative predictions about the structure of the magnetotail

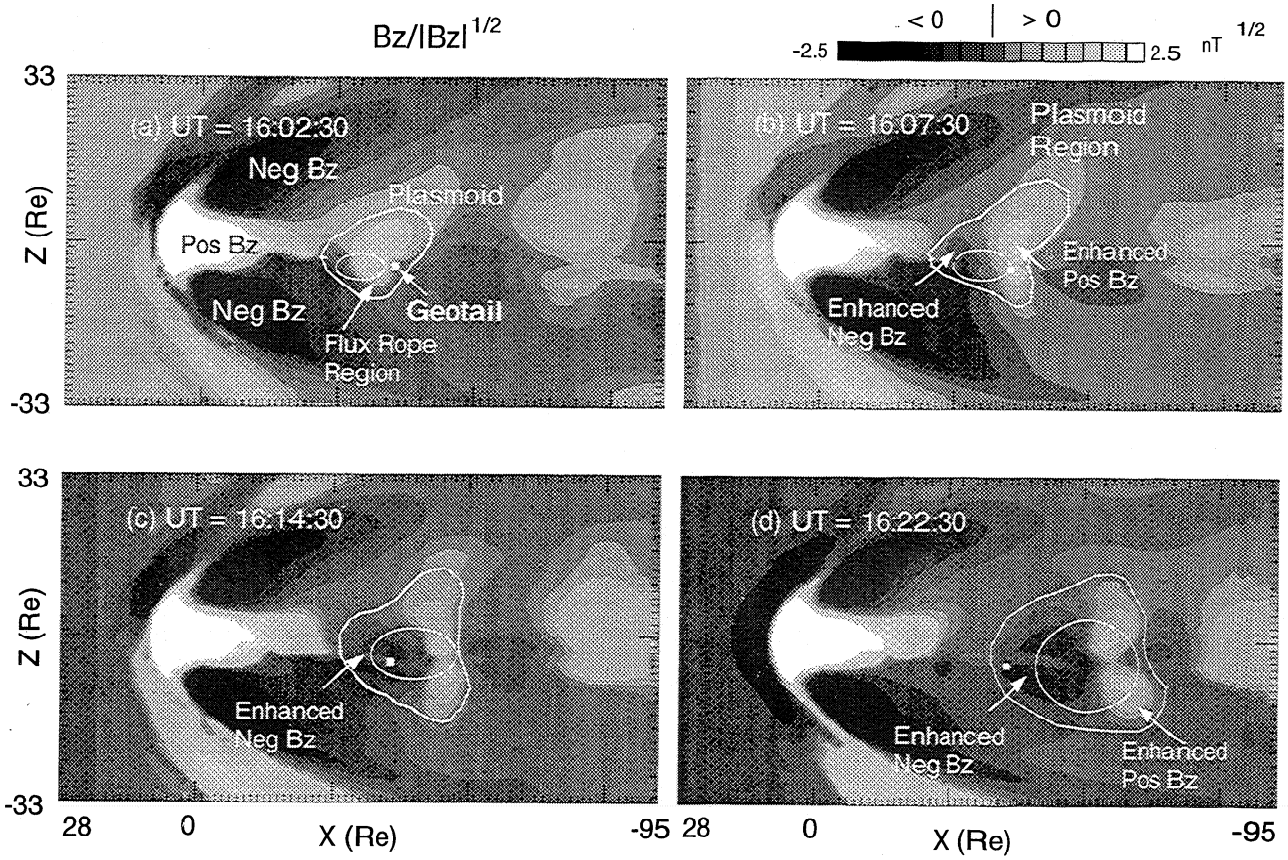

Figure 12. As in Figure 11, except B_z is shown. The plasmoid is identified by the bipolar signature in B_z. The cross-sectional area of the plasmoid is seen to be much larger than the flux rope signature.

during active periods. Most of the reconnection events, both modeled and observed, are associated with strong core magnetic fields, i.e., flux ropes. They are generated earthward of Geotail at about $x \simeq -20 R_E$ and arrive at Geotail about 10 min later. This timing implies that they are generated almost simultaneously with observed ionospheric disturbances.

The core magnetic fields that are generated by the above corrections to Ohm's law are highly localized structures (2-4 R_E) with a distinctive bipolar feature. In the present case when the spacecraft is on the dusk-side, the leading (or tailward) half tends to have positive B_y that is strongest in the northern hemisphere. The trailing or earthward half has negative B_y which is strongest in the southern hemisphere. As the flux rope moves down the tail, its cross-sectional size increases due to expansion from a few R_E to 10-15 R_E, consistent with previous observations. In addition, the core field of the leading portion tends to weaken, so that the most intense core field tends to be in the same direction as B_y IMF, also consistent with observations.

The probability of whether a spacecraft observes a unidirectional or bipolar signature depends on how close the spacecraft approaches the center of the current sheet and how far it is down the tail. In the near-Earth region, bipolar signatures are most likely to be observed when the spacecraft is close to the center of the current sheet, while unidirectional signatures are predicted to be more common when the spacecraft is at a distance greater than 1-2 R_E from the center of the current sheet. The probability of detecting a bipolar signature is expected to decrease down the tail due to the reduction of the core field in the leading edge. The spatial dependence is consistent with the fact that unidirectional B_y signatures are more often observed than bipolar signatures. Of the four events presented here, one was observed to have a bipolar signature. However, there were additional bipolar signatures present in the data shown in Figure 3.

The first two negative B_z or reconnection case studies occurred during the first half of the day when the ionospheric activity was relatively quiet. These events could be directly related to changes in the IMF conditions, and the resultant propagation of the negative B_z from the dayside into the nightside could be traced in the model. These events are therefore externally triggered. They involved reconnection along field lines that were initially closed in the model. The third case study indicated reconnection in the vicinity of a "Y" reconnection region, when IMF B_z was either zero or weakly southward. Under these conditions the enhanced reconnection that produces the observed negative B_z events

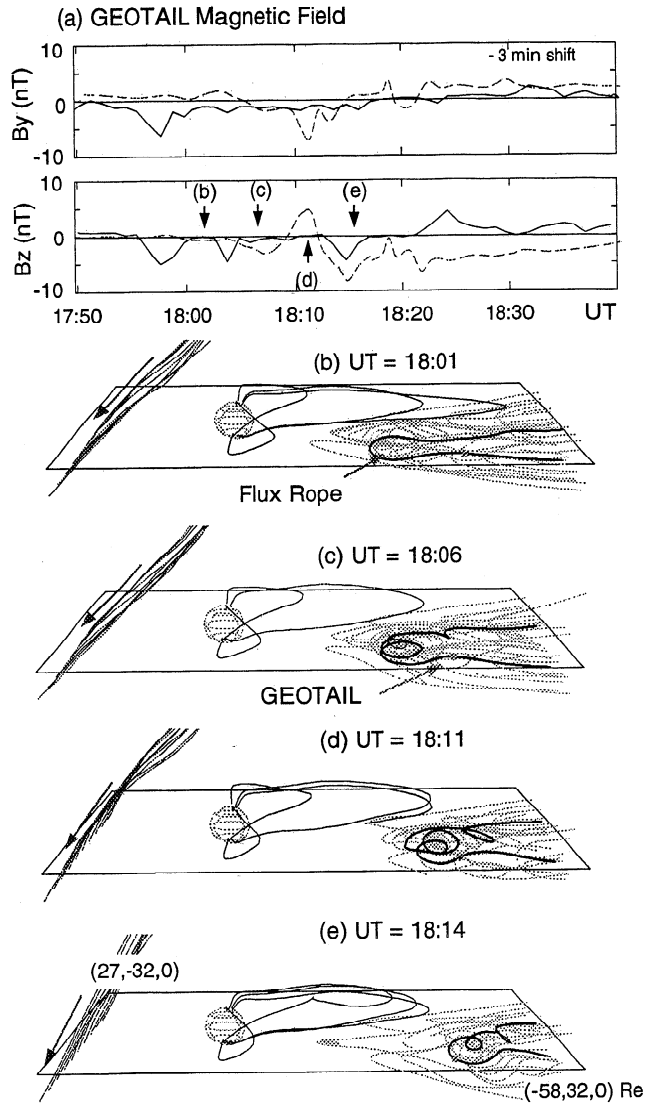

Figure 13. A multiple reconnection event. Flux ropes with negative B_y are still seen, even though B_y IMF has been positive for the preceding 2 hours. The predicted structure appears more consistent with the first spikes observed by 1758 UT rather than with the last negative B_z spike when it actually appears. Nevertheless, the conclusions are the same in that small-scale structures are being generated in a preexisting shallow (only weakly negative B_z) neutral point.

can be initiated by subtle changes in the global IMF conditions which may enhance local convection and allow kinetic processes to drive the reconnection. In the fourth case, the IMF B_z was strongly southward and local processes allow multiple reconnection to occur. In the latter case, relatively large (-5 nT) negative B_z events are also observed.

Thus, both local and global triggering of tail reconnection processes appear to be possible. Local triggering is not well incorporated in global MHD because it does not fully incorporate small-scale kinetic processes. The present model incorporates some of these processes but clearly is not all-inclusive. The fact that nonideal MHD processes can modify the structure of the reconnection site and the dynamics of the tail, even with the limited treatment presented here, is indicative of the importance of the simultaneous inclusion of both local and global processes. This interplay is further highlighted by the fact that the largest negative B_z events observed by Geotail tend to have the smallest timescale and the largest amount of fine structure.

Acknowledgments. Support for the 3D Plasma and Energetic Particle investigation was provided by NASA grant NAS5-2815 at the University of California, Berkeley, and by NASA grant NAG5-2813 to the University of Washington. The simulations were supported by National Science Foundation grant ATM-9321665 and NASA grant NAGW-5047 to the University of Washington and by the Cray C-90 at the San Diego Supercomputing Center which is supported by the National Science Foundation. The authors also wish to thank Y. Saito and T. Yamamoto for assistance in processing the Geotail magnetic field and plasma data, and G. Rostoker for providing data from CANOPUS which was constructed by and is maintained and operated by the Canadian Space Agency.

The Editor thanks S. W. Cowley and W. J. Hughes for their assistance in evaluating this paper.

References

Birn, J., and M. Hesse, The magnetic topology of the plasmoid flux rope in a MHD-simulation of magnetotail reconnection, in *Physics of Magnetic Flux Ropes, Geophys. Monogr. Ser.*, vol. 58, edited by C. T. Russell, E. R. Priest, and, L. C. Lee, p. 655, AGU, Washington, D.C., 1990.

Biskamp, D., E. Schwartz, and J. F. Drake, Ion-controlled collisionless magnetic reconnection, *Phys Rev. Lett., 75*, 3850, 1995.

Cattell, C. A., and F. S. Mozer, Substorm electric fields in the Earth's magnetotail, in *Magnetic Reconnection in Space and Laboratory Plasmas*, Geophys. Monogr. Ser., vol. 30, edited by E. W. Hones, Jr., p. 208, AGU, Washington, D.C., 1984.

Drake, J. F. R. G. Kleva,, and M. E. Mandt, Structure of thin current layers: Implications for magnetic reconnection, *Phys Rev. Lett., 73*, 1251, 1994.

Elphic, R. C., C. A. Cattell, K. Takahashi, S. T. Bame, and C. T. Russell, ISEE-1 and 2 observations of magnetic flux ropes in the magnetotail: FTE's in the plasma sheet? *Geophys. Res. Lett., 13*, 648, 1986.

Fu, Z. F., L. C. Lee, and Y. Shi, A three-dimensional MHD simulation of the multiple X line reconnection process, in *Physics of Magnetic Flux Ropes, Geophys. Monogr. Ser.*, vol. 58, edited by C. T. Russell, E. R. Priest, and, L. C. Lee, p. 515, AGU, Washington, D.C., 1990.

Hones, J. W., Jr., The magnetotail: Its generation and dissipation, in *Physics of Solar Planetary Environments*, edited D. J. Williams, p. 559, AGU, Washington, D.C., 1976.

Hones, J. W., Jr., Plasma flows in the magnetotail and their relation to substorms theories, in *Dynamics of the Magnetosphere*, edited S. I. Akasofu, p. 545, D. Reidel, Norwell, Mass., 1979.

Kivelson, M. G., K. K. Khurana, R. J. Walker, L. Kepko, and D. Xu, Flux ropes, interhemispheric conjugacy, and magnetospheric current closure, *J. Geophys. Res., 101*, 27,341, 1996.

Krall, N. A., and A. W. Trivelpiece, *Principles of Plasma Physics*, San Francisco Press, Inc., San Francisco, 1986.

Lepping, R. P., D. H. Fairfield, J. Jones, L. A. Frank, W. R. Paterson, S. Kokubun, and T. Yamamoto, Cross-tail magnetic flux ropes as observed by the Geotail spacecraft, *Geophys. Res. Lett., 22*, 1193, 1995.

Lepping, R. P., J. A. Slavin, M. Hesse, J. A. Jones, and A. Szabo, Analysis of magnetotail flux ropes with strong core fields: ISEE 3 observations, *J. Geomagn. Geoelectr., 48*, 589, 1996.

Ma, Z. W., and A. Bhattacharjee, Fast impulsive reconnection and current sheet intensification due to electron pressure gradients in semi-collisional plasmas, *Geophys. Res. Lett., 23*, 1673, 1996.

Moldwin, M. B., and W. J. Hughes, On the formation and evolution of plasmoids: A survey of ISEE 3 Geotail data, *J. Geophys. Res., 97*, 19,259, 1992.

Ogino, T., R. J. Walker, and M. Ashour-Abdalla, Magnetic flux ropes in 3-dimensional MHD simulations, in *Physics of Magnetic Flux Ropes*, *Geophys. Monogr. Ser.*, vol. 58, edited by C. T. Russell, E. R. Priest, and, L. C. Lee, p. 669, AGU, Washington, D.C., 1990.

Pritchett, P. L.,, F. V. Coroniti, and V. K. Decyk, Three-dimensional stability of thin quasi-neutral current sheets, *J. Geophys. Res., 101*, 27,413, 1996.

Sibeck, D. G., Evidence for flux ropes in the Earth's magnetotail, in *Physics of Magnetic Flux Ropes*, *Geophys. Monogr. Ser.*, vol. 58, edited by C. T. Russell, E. R. Priest, and L. C. Lee, p. 637, AGU, Washington, D.C., 1990.

Sibeck, D.G., G. L. Siscoe, J. A. Slavin, E. J. Smith, S. J. Bame, and F. L. Scarf, Magnetotail flux ropes, *Geophys. Res. Lett., 11*, 1090, 1984.

Slavin, J. A., et al. , CDAW-8 observations of plasmoid signatures in the geomagnetic tail: An assessment, *J. Geophys. Res., 94*, 15,153, 1989.

Slavin, J. A., C. J. Owen, M. Kuznetsova, and M. Hesse, ISEE 3 observations of plasmoids with flux rope magnetic topologies, *Geophys. Res. Lett., 22*, 2061, 1995.

Steinolfson, R. S., and R. M. Winglee, Energy storage and dissipation in the magnetotail during substorms, 2., MHD simulations, *J. Geophys. Res., 98*, 7536, 1993.

Winglee, R. M., Non-MHD influences on the magnetospheric current system, *J. Geophys. Res., 99*, 13,437, 1994.

Winglee, R. M., and R. S. Steinolfson, Energy storage and dissipation in the magnetotail during substorms, 1., Particle simulations, *J. Geophys. Res., 98*, 7519, 1993.

Winglee, R. M., V. O. Papitashvili, and D. R. Weimer, Comparison of the high latitude ionospheric electrodynamics inferred from global simulations and semi-empirical models for the January 1992 GEM campaign, *J. Geophys. Res.*, in press, 1997a.

Winglee, R. M., R. M. Skoug, R. P. Lin, R. L. Lepping, T. Mukai, T. Terasawa, S. Kokubun, H. Reme, and T. Sanderson, IMF induced changes in the nightside magnetosphere using Wind/Geotail/IMP 8 Observations and Modeling, *Geophys. Res. Lett.*, in press, 1997b.

Winglee, R. M., R. M. Skoug, A. T. Y. Lui, R. P. Lin, R. L. Lepping, S. Kokubun, G. Rostoker, and J. C. Samson, Magnetospheric/Ionospheric Activity During an Isolated Substorm: A Comparison between Wind/Geotail/IMP 8/CANOPUS Observations and Modeling, *Encounter Between Global Observations and Models in the ISTP Era*, Geophys. Monograph, AGU, in press, 1997c.

Zhu, Z., and R. M. Winglee, Tearing instability, flux ropes, and the kinetic current sheet kink instability in the Earth's magnetotail: A three-dimensional perspective from particle simulations, *J. Geophys. Res., 101*, 4885, 1996.

S. Kokubun, STELAB, Nagoya University, 3-13 Honohara Toyokawa, Aichi 442, Japan.

R. P. Lepping, Code 695, NASA Goddard Space Flight Center, Greenbelt, MD 20771.

R. P Lin, Space Sciences Laboratory, University of California, Berkeley, CA 94720.

R. M. Winglee, Geophysics Program, Box 351650, University of Washington, Seattle WA 98195-1650.

(Received March 13, 1997; revised August 22, 1997; accepted August 22, 1997.)